PFC/JA-81-3

Analytic Theory of a Tapered Gyrotron Resonator

R. J. Temkin

February 1981

Analytic Theory of a Tapered Gyrotron Resonator *

R. J. Temkin

Plasma Fusion Center †
Massachusetts Institute of Technology
Cambridge, Massachusetts 02139

* Work supported by U.S.D.O.E. Contract DE-AC02-78ET-51013

† Supported by U.S. Department of Energy

Abstract

An analytic theory has been derived for determining the eigenfrequencies, RF-field distribution and Q of the TE_{mpq} modes of a gyrotron resonator consisting of a circular cylinder joined to a slowly tapered section. Explicit results are obtained for a linear taper. The cavity modes are found to have an RF-field distribution which is useful for prebunching the electron beam and enhancing efficiency. For high Q cavities, the cavity Q depends on axial mode number q as q^{-2}, which is important for mode discrimination. Proper selection of taper length is found to reduce the Q of high q modes, also aiding in mode discrimination. The present approach may be applied to other forms of weakly irregular cavities, such as cavities with nonlinear tapers.

1. Introduction

In recent years, the gyrotron has proven to be an impressive source of high power, millimeter wave radiation (1,2,3). One important problem in gyrotron research is the design of cavities which optimize the gyrotron output efficiency and provide good discrimination between adjacent cavity modes. Vlasov et al. (4) have suggested the use of open resonators consisting of segments of weakly irregular waveguide. These and similar structures have found extensive application in the design of practical gyrotron devices (1-8).

In this papèr, we present an analytic solution for the eigenfrequencies, quality factor (Q) and RF field distribution for the TE modes of a cylindrical cavity consisting of a straight section joined onto a tapered section. These solutions illustrate the dependence of the resonator properties on the fundamental cavity parameters, such as the length and radius of the straight section and the taper angle. The present results allow a simple comparison between the properties of tapered and untapered resonators. The results should find direct application in design of gyrotron resonators.

2. Analytic Resonator Theory

The resonator configuration for which explicit results will be obtained is illustrated in Fig. 1. The resonator consists of two sections, a straight section and a tapered section. In the present treatment, the straight section will be assumed to have a circular cross-section of radius R_o, length L. The tapered section will be assumed to taper linearly, forming a cone, so that the resonator radius can be expressed as:

$$R(z) = \begin{cases} R_o & z_o \leq z \leq z_o + L \\ R_o + (z - z_o) \tan\theta & z_o - (R_o/\tan\theta) \leq z \leq z_o \end{cases} . \tag{1}$$

Although a circular cross-section and a linear taper have been assumed in the present analysis, the present approach can be extended to non-circular cross-sections and non-linear tapers.

The present solutions will utilize the transmission line approach to the solution of the wave equation in the resonator (1,9,10,11). The tapered section will be considered to consist of many segments, in each of which the wave equation

$$(\nabla^2 + k^2)\, \vec{E}(r,\theta,z) = 0 \tag{2}$$

$$kc = \omega$$

is locally satisfied. In each segment, the TE modes may be represented by (12,13)

$$\vec{E}(r,\theta,z) = \vec{E}_t(r,\theta)\, E_\ell(z)$$

where
$$\vec{E}_t(r,\theta) = \hat{z} \times \nabla_\perp \Psi(r,\theta)$$
$$\left(\nabla_\perp^2 + k_\perp^2(z)\right) \Psi(r,\theta) = 0 \qquad (3)$$

and
$$\left(\frac{d^2}{dz^2} + k_\parallel^2\right) E_\ell(z) = 0$$
$$k_\parallel^2 = k^2 - k_\perp^2(z) \qquad (4)$$

For the circular cross-section resonator assumed here, the transverse field structure is given by the usual Bessel functions (12) and

$$k_\perp(z) = \nu_{mp}/R(z)$$

where $R(z)$ is given by Eq.(1) and ν_{mp} is the p^{th} root of $J'_m(x) = 0$. The solutions of Eqs.(3) and (4), together with the boundary conditions, yield the eigenfrequencies ω_{mpq} of the TE_{mpq} modes of the resonator. In the present analysis, we ignore the dispersive effects due to the presence of an active medium in the resonator (if any) or due to the ohmic Q of the resonator, which is assumed large. We also assume that only a single mode is excited in the cavity.

The solutions of Eq.(4) can be obtained in the three regions labelled I, II and III in Fig. (1). The point $z = 0$ is defined, for convenience, as the location at which $k_\parallel(z)$ is zero, that is the turning point of the wave. The location of the turning point, as well as the distance z_o, will differ for each mode (mpq).

In the straight section, region III, the solution of the longitudinal wave equation, Eq.(4), is given by:

$$E_3(z) = A_{3+}\, E_{3+} + A_{3-}\, E_{3-}$$

$$E_{3\pm}(z) = k_{\|,0}^{-1/2} \exp(\pm\, i\, k_{\|,0}\, z)$$

$$k^2 = k_{\perp,0}^2 + k_{\|,0}^2 = (2\pi/\lambda)^2 \tag{5}$$

$$k_{\perp,0} = \nu_{mp}/R_o$$

Thus, a solution for $k_{\|,0}$ also yields a solution for $k = \omega/c$.

In the tapered section, we may write $k_{\|}(z)$ as:

$$k_{\|}^2(z) = k^2 - \frac{\nu_{mp}^2}{R_0^2 \left(1 + \frac{(z - z_0)\tan\theta}{R_0}\right)^2} \tag{6}$$

The condition $k_{\|}(z = 0) = 0$ yields:

$$z_o = \frac{R_o}{\tan\theta}\left(1 - \frac{k_{\perp,0}}{k}\right) \tag{7}$$

Near $z = 0$, we may approximate Eq.(6) by:

$$k_{\|}^2(z) = k_{\|,0}^2 + \frac{2\,\nu_{mp}^2\,\tan\theta}{R_0^3}(z - z_o) \tag{8}$$

Eq.(8) is valid so long as:

$$\frac{z_0\,\tan\theta}{R_0} \ll 1$$

This last inequality also insures that the turning point, $z = 0$, occurs

well before the radius of the tapered section goes to zero. Using Eq.(7), this condition can be rewritten:

$$1 - (k_{\perp,0}/k) << 1 \tag{9}$$

or

$$\frac{q^2 \lambda^2}{8L^2} \approx \frac{q^2 \pi^2 R_0^2}{2 \nu_{mp}^2 L^2} << 1$$

For gyrotron resonators, the optimum efficiency is generally achieved in resonators with waves near cutoff (1), for which Eq.(9) is accurate. Therefore, we shall employ the approximation in Eq.(8) throughout region II.

In region I, the wave equation is written using:

$$\kappa_{\|}^2 (z) = \frac{\nu_{mp}^2}{R_0^2 \left(1 + \frac{(z - z_0) \tan\theta}{R_0}\right)^2} - k^2 \tag{10}$$

which, for $-z_0 \leq z \leq 0$, may be rewritten

$$\kappa_{\|}^2 (z) = \frac{2 \nu_{mp}^2 \tan\theta}{R_0^3} (z_0 - z) - k_{\|,0}^2 \tag{11}$$

Finally, it should be noted that the definition $k_{\|}(0) = \kappa_{\|}(0) = 0$, when applied to Eqs.(8) and (11), yields:

$$z \approx \frac{k_{\|,0}^2 R_0^3}{2 \nu_{mp}^2 \tan\theta} \tag{12}$$

Eq.(12) may be shown to be accurate so long as Eq.(9) is satisfied. We may use Eq.(12) to rewrite Eqs.(8) and (11). Before doing so, we introduce

the dimensionless "irregularity" parameter ξ, which was utilized by Vlasov et al. (4):

$$\xi = \nu_{mp}^2 \, L^3 \, \tan\theta/8 \, R_0^3 \approx \nu_{mp}^2 \, L^3 \, \theta/8 \, R_0^3 \tag{13}$$

For a cavity near cutoff, ξ may also be written as:

$$\xi \approx \pi^3 \, L^3 \, \theta/\nu_{mp} \, \lambda^3 \tag{14}$$

Fig. 2 illustrates the range of values of ξ vs. θ for several values of L/λ and for a TE_{02q} mode. Using ξ, we obtain:

$$\begin{aligned} k_{\|}^2(z) &= 16 \, \xi \, L^{-3} \, z \, . \qquad 0 \leq z \leq z_0 \\ \kappa_{\|}^2(z) &= 16 \, \xi \, L^{-3} \, |z| \qquad -z_0 \leq z \leq 0 \end{aligned} \tag{15}$$

Using Eq.(15) in the wave equation (4), we may obtain solutions for $E_\ell(z)$. These solutions will be written in a more general form, familiar from WKB theory (14), which will be more useful for treating other problems, such as nonlinear tapers. Define

$$\begin{aligned} \eta_2(z) &= \int_0^z k_{\|}(z') \, dz' \qquad 0 \leq z \leq z_0 \\ \eta_1(z) &= \int_0^{|z|} \kappa_{\|}(z') \, dz' \qquad -z_0 \leq z \leq 0 \end{aligned} \tag{16}$$

In the present case,

$$\begin{aligned} \eta_2(z) &= \frac{8}{3} \xi^{1/2} \, L^{-3/2} \, z^{3/2} \\ \eta_1(z) &= \frac{8}{3} \xi^{1/2} \, L^{-3/2} \, |z|^{3/2} \end{aligned} \tag{17}$$

Then the solutions for $E_\ell(z)$ in region II can be written in the form:

$$E_2(z) = A_+ E_{2+}(z) + A_- E_{2-}(z)$$
$$E_{2\pm}(z) = \eta_2^{1/2} k_{||}^{-1/2} J_{\pm\frac{1}{3}}(\eta_2) \tag{18}$$

while in region I the solutions are written:

$$E_1(z) = B_+ E_{1+}(z) + B_- E_{1-}(z)$$
$$E_{1\pm}(z) = \eta_1^{1/2} \kappa_{||}^{-1/2} I_{\pm\frac{1}{3}}(\eta_1) \tag{19}$$

where J and I are Bessel functions and $A_\pm$, $B_\pm$ are constants. Eqs.(5), (18) and (19) represent the solution for the RF field axial distribution. To obtain explicit results, the boundary conditions must be imposed. The boundary conditions consist of properly joining the E-field distribution and its derivative between regions, requiring a specified reflection at $z = z_0 + L$ and requiring a decaying wave in the region $z << 0$.

The boundary conditions at $z = 0$ are obtained using:

$$J_{\pm\frac{1}{3}}(\eta_2) \xrightarrow[z \to 0]{} \frac{\left(\frac{1}{2}\eta_2\right)^{\pm\frac{1}{3}}}{\Gamma\left(1 \pm \frac{1}{3}\right)}$$

$$I_{\pm\frac{1}{3}}(\eta_1) \xrightarrow[z \to 0]{} \frac{\left(\frac{1}{2}\eta_1\right)^{\pm\frac{1}{3}}}{\Gamma\left(1 \pm \frac{1}{3}\right)}$$

which then requires $B_+ = -A_+$ and $B_- = A_-$. Furthermore, to obtain a pure decaying wave as $z \to -\infty$, we require $A_+ = A_- = A$. Then the appropriate wave functions are:

$$E_2(z) = A\,(E_{2+}(z) + E_{2-}(z))$$

$$E_2(z) = A\,(E_{1-}(z) - E_{1+}(z))$$

$$E_1(0) = E_2(0)$$

$$E_2(z) = A\left(\frac{6}{\pi k_{||}}\right)^{1/2} \cos\left(\eta_2 - \frac{\pi}{4}\right) \qquad z \to \infty$$

$$E_2(z) = A\left(\frac{\eta_2}{k_{||}}\right)^{1/2}\left(\frac{\eta_2^{1/3}}{2^{1/3}\,\Gamma\left(\frac{4}{3}\right)} + \frac{2^{1/3}}{\eta_2^{1/3}\,\Gamma\left(\frac{2}{3}\right)}\right) \qquad z \to 0 \qquad (20)$$

$$E_1(z) = \frac{1}{2} A\left(\frac{6}{\pi\kappa_{||}}\right)^{1/2} e^{-\eta_1} \qquad z \to -\infty$$

To join the solution for $E_2(z)$ to that for $E_3(z)$ at $z = z_0$, it is necessary to match the fields and their first derivatives at that point. This can be done easily if the value of ξ is not too large. To prove this, we consider a wave $\exp(-i k^{*}_{||,0} z)$ travelling towards $(-z)$ in the straight section. For small ξ, the wave undergoes a very weak reflection at $z = z_0$. The transmitted wave then travels down the tapered section to $z = 0$, where it is turned around, propagating back to the straight section. If the reflectivity at $z = z_0$ is small, the weak wave reflected at $z = z_0$ can be ignored relative to the wave turned around at $z = 0$. By contrast, for very large ξ, the wave will be almost completely reflected at $z = z_0$, so that the wave returning after being turned around in the tapered portion of the cavity can be ignored.

This argument can be quantified as follows. By equating E_2 and E_3 and their derivatives at $z = z_0$, we obtain for the reflection coefficient, R_j, (a similar problem has been considered by Vaynshtein (11)):

$$R_j = - \frac{1 - ik_{\|,0} \frac{E_2(z_0)}{E_2'(z_0)}}{1 + ik_{\|,0} \frac{E_2(z_0)}{E_2'(z_0)}}$$

For small ξ, $E_2(z_0)$ is evaluated in the limit of large z, yielding

$$R_j = \frac{i\, k_{\perp,0}^2 \tan\theta}{4\, k_{\|,0}^3 R_o} = \frac{i\, 2\xi}{k_{\|,0}^3 L^3} \tag{21}$$

For large ξ, $E_2(z_0)$ is evaluated in the limit of small z using Eq.(20), yielding

$$R_j \approx \exp\left(2i\, \beta_o\, e^{i\pi/3} (k_{\|,0}\, z_0)^{1/3}\right) \tag{22}$$

where

$$\beta_o = \frac{3^{2/3}\, \Gamma\left(\frac{4}{3}\right)}{\Gamma\left(\frac{2}{3}\right)} = 1.370$$

For large ξ,

$$|R_j| \approx 1 - \frac{\sqrt{3}\, \beta_o\, k_{\|,0}\, L}{2\, (2\xi)^{1/3}} \approx 1$$

When the reflectivity at the junction between the straight section and the tapered section becomes large, an additional aspect of the problem, namely mode conversion, should be considered.

For the present, we shall assume that ξ is sufficiently small that reflection and mode conversion in the taper region may be ignored. At a later point, we may establish the range of values of ξ for which this approximation is valid.

Since $E_2(z)$ can be represented as having a cosine distribution for large $\eta_2(z)$, which occurs at large z, it may be joined to the waves $\exp(\pm ik_{||,0}\, z)$ in the straight section if reflections at $z = z_0$ are ignored. A particulary simple result is obtained when the resonator is terminated at $z = z_0 + L$ by a reflecting wall, which yields a purely real reflection coefficient $R = -1$ and forces $E_3(z_0 + L)$ to be zero. Then, we may extend the definition of $\eta_2(z)$:

$$\eta_2(z) = \begin{cases} \frac{8}{3}\xi^{1/2}\, L^{-3/2}\, z^{3/2} & 0 \leq z \leq z_0 \\ \frac{1}{24}\frac{k_{||,0}^3\, L^3}{\xi} - k_{||,0}(z - z_0) & z_0 \leq z \leq z_0 + L \end{cases} \tag{23}$$

The boundary condition at $(z_0 + L)$ requires $\cos(\eta_2 - \pi/4)$ to be zero, which, using Eq.(23), yields

$$k_{||,0}\, L + \frac{k_{||,0}^3\, L^3}{24\,\xi} = \pi\left(q - \frac{1}{4}\right) \tag{24}$$

where $q = 1,2,3$, etc. Eq.(24) is the dispersion relation for the cavity of Fig. (1) with a reflecting wall at $(z_0 + L)$. Since Eq.(24) is a cubic equation, it may be easily solved for $k_{||,0}\, L$. The value of $k_{||,0}$, combined with $k_{\perp,0} = \nu_{mp}/R_0$, yields k and ω.

Eq.(24) may also be derived from a different point of view. Consider a wave $\exp(ik_{||,0}\, z)$ travelling in the straight section toward the reflecting output coupler. This coupler could be an iris, a tapered output waveguide, a strip grating or other component. We assume, however, that the reflection occurs at $z = z_0 + L$ and that there is no mode

conversion. The reflectivity is given by

$$R = |R|\ e^{i\phi_R}$$

The reflected wave propagates back to the turning point, $z = 0$, where it is turned around with an effective phase change of $(\pi/2)$. The cumulative phase change in a round trip must be 2π times an integer (q) so that:

$$\int_0^{z_0+L} k_{||}\,(z)\,dz + \phi_R + \int_0^{z_0+L} k_{||}\,(z)\,dz - \frac{\pi}{2} = 2\pi q$$

This leads to a dispersion relation:

$$\int_0^{z_0+L} k_{||}(z)\,dz = \pi\left(q + \frac{1}{4}\right) - \frac{\phi_R}{2} \qquad (25)$$

For a reflection from a metallic wall ($\phi_R = \pi$) and a linear taper, Eq.(25) reduces to Eq.(24).

For the cavity of Fig. 1, the Q will primarily depend on the radiation transmitted through the partially reflecting mirror at $z = z_0 + L$. Ohmic losses and losses due to mode conversion will be neglected. Also, the taper length in the $(-z)$ direction is assumed to be sufficiently long that radiation in the mode of interest does not tunnel out of the cavity in the $(-z)$ direction. For large negative values of z, the RF fields fall off as

$$E_i(z) \sim \frac{1}{\kappa_{||}^{1/2}}\, e^{-\eta_i(z)}$$

where $\kappa_{||}(z)$ is given by Eq.(15) and $\eta_i(z)$ by Eq.(17). The 1/e falloff occurs in an axial distance of about $0.5\,\xi^{-1/3}\,L$, so that the taper length beyond $z = 0$ must significantly exceed this distance.

The resonator Q is defined as (15)

$$Q \equiv \frac{\omega U}{dU/dt} = \omega t_c \qquad (26)$$

where U is the stored energy and t_c the cavity decay time. The cavity decay time may be expressed in terms of the transit time and output coupling parameters (13). Assuming that there are no losses at the taper end,

$$t_c \cong \frac{1}{-\ell n|R|} \int_0^{z_0+L} \frac{dz}{v_{gr}} \qquad (27)$$

$$v_{gr} = \frac{d\omega}{dk_{||}} = \frac{k_{||}c}{k}$$

Using Eq.(15) for $k_{||}(z)$ between $0 \leq z \leq z_0$ and using $k_{||} = k_{||,0}$ in the straight section, Eq.(27) yields:

$$Q = 4\pi \left(\frac{L}{\lambda}\right)^2 \left(\frac{\pi}{k_{||,0}\, L}\right) \left(1 + \frac{k_{||,0}^2\, L^2}{8\xi}\right) \left(-\frac{1}{\ell n|R|}\right) \qquad (28)$$

In the limit where $|R|$ tends to unity, this may be written:

$$Q \approx 4\pi \left(\frac{L}{\lambda}\right)^2 \left(\frac{\pi}{k_{||,0}\, L}\right) \left(1 + \frac{k_{||,0}^2\, L^2}{8\xi}\right) \left(\frac{1}{1 - |R|}\right) \qquad (29)$$

Eq.(29) has an error of less than 10% for $|R| \gtrsim 0.8$. For smaller values of $|R|$, Eq.(28) applies. In the limit $|R| \to 0$, which corresponds to a mirrorless or superradiant oscillator, Eq.(28) yields $Q \to 0$. However, the limit $Q = 0$ is not reached since radiation generated in the cavity requires a finite t_c to travel out of the cavity. In fact, Q becomes small but nonzero as $|R| \to 0$.

3. Results

For the cavity of Fig. 1, the oscillation frequency, $\omega = kc$, may be obtained from the value of $k_{\perp,0} = \nu_{mp}/R_o$ and the value of $k_{||,0}$. Solutions for $k_{||,0}$ for a phase shift of $\phi_R = \pi$ are obtained from Eq.(24) and plotted in Fig. 3 for a $q = 1$ mode and Fig. 4 for a $q = 2$ mode. To obtain explicit results for the cavity Q using Eq.(28), we must know the value of $k_{||,0}L$ vs. ξ. For illustrative purposes, we will assume that the output mirror is highly reflecting, that is, $1 - |R|$ is small and ϕ_R is close to π. Then $k_{||,0}L$ vs. ξ is given by Eq.(24). The resulting values of cavity Q vs. ξ, using Eqs.(24) and (28), are plotted in Fig. 3 for a $q = 1$ mode and Fig. 4 for a $q = 2$ mode. The results for Q in Figs(3) and (4) must be divided by $(-\ln|R|)$ to account for the finite reflectivity at $z = z_o + L$. Both $k_{||,0}L$ and $Q\,\lambda^2 L^{-2}$ are functions only of the axial mode number, q, and the irregularity parameter, ξ.

With decreasing ξ, $k_{||,0}\,L$ decreases to zero (as $\xi^{1/3}$) while Q increases (as $\xi^{-1/3}$). As ξ decreases, the wave travelling from the straight section into the tapered section penetrates an increasingly greater distance before being turned around. This increases the effective cavity length and thus increases the cavity Q and decreases the axial wavenumber, $k_{||,0}$.

For large ξ, $k_{||,0}\,L$ increases to $(q - 0.25)\,\pi$ and Q decreases to Q_{MIN} divided by $(q - 0.25)$, where Q_{MIN} is $4\pi\,L^2\,\lambda^{-2}$. These values differ from those for an untapered cavity, for which $k_{||,0}\,L$ equals $q\pi$ and Q equals Q_{MIN} divided by q. However, as described in the previous section, Eqs.(24) and (28) are not valid for large ξ because they do not account

for reflections at the junction of the tapered and straight sections. The limits of validity of the equations may now be estimated as follows. For small ξ, the reflection at the junction is given by Eq.(21),

$$|R_j| \approx \frac{2\xi}{k_{||,0}^3 L^3}$$

Then $|R_j|$ will be small so long as:

$$\begin{aligned} \xi &\lesssim 5 \qquad q = 1 \\ \xi &\lesssim 70 \qquad q = 2 \end{aligned} \qquad |R_j| << 1.$$

Thus, the results in Fig. (3) and Fig. (4) only apply in this range of ξ. On the other hand, Eq.(22) indicates that the reflection will be large so long as:

$$\begin{aligned} \xi &\gtrsim 40 \qquad q = 1 \\ \xi &\gtrsim 500 \qquad q = 2 \end{aligned} \qquad |R_j| \approx 1.$$

For ξ large enough so that $|R_j| \approx 1$, the wave will be reflected at $z = z_0$. Consequently, for ξ larger than these values, $k_{||,0} L \approx q\pi$ and $Q(-\ell n|R|) \approx q^{-1} Q_{MIN}$. Thus, for large ξ, the taper acts as a mirror, as expected.

Fig. 5 is a comparison of the results for a q = 1 and a q = 2 mode. The quantities plotted vs. ξ are $\Delta\omega$, the frequency difference between the q = 1 and q = 2 modes, and the ratio of the Q of the q = 1 and q = 2 modes. The reflectivity, R, has been assumed to be independent of q. For comparison, for a straight cylinder of length L, $(\Delta\omega/\omega)$ equals $(3\lambda^2/8L^2)$ and the ratio $Q(q = 1)/Q(q = 2)$ equals 2. Both the relative Q and the frequency separation can be very greatly altered by

the dependence of the output reflectivity, R, on q, as well as by the effect of a finite taper length. This is discussed in the next section.

Fig. 6 gives examples of the axial distribution of the RF field amplitude for q = 1 and 2 and for ξ = 0.5 and 5.0. As expected, with decreasing ξ the wave penetrates farther into the tapered section. However, an important result is that the q = 2 wave, being farther from cutoff than the q = 1 wave, penetrates a greater distance into the taper than the q = 1 wave. This arises because the distance along the taper to the turning point, z_0, depends on $k_{\|,0}^2$. This can be used to advantage in mode discrimination, particularly when combined with other mode discrimination techniques. If the taper angle is small and the taper length is adjusted so as to just allow the q = 1 mode to be attenuated, the q = 2 and higher modes may be able to tunnel out of the taper. This can lower the Q of these modes and lead to suppression of the higher order axial modes. On the other hand, this same analysis indicates that it could be dangerous under certain conditions to excite higher order axial modes in high power gyrotrons. Gyrotrons with very high power beams can excite low Q modes, such as higher order axial modes. If the resonator taper is designed to just cutoff the q = 1 mode, and a higher q mode is accidentally excited, high power radiation could be emitted toward the electron gun section of the tube.

4. Discussion

Cavities made up of weakly irregular sections of waveguide can have several advantages over a straight, circular cylinder cavity. These advantages include an axial RF field structure leading to increased efficiency and an improved separation of modes in frequency and Q. This section describes the degree to which simple tapered cavities achieve these goals.

The efficiency of a gyrotron is known to be improved when the electrons enter an interaction region in which a weak, spatially extended RF field acts to initiate the electron bunching (1,5,16). Since an RF field with a Gaussian profile has such a prebunching region, while a sinusoidal distribution does not, the former is found to be more efficient than the latter (17). Cavities which taper down in diameter toward the electron gun have an axial RF field amplitude which slowly decreases with distance into the taper and becomes Gaussian-like beyond the turning point. The exponential decay beyond the turning point is a general feature of WKB theory, as evidenced by the form of $E_1(z)$, Eq.(19). Therefore, weakly tapered cavities, with linear or nonlinear tapers, should, in general, provide enhanced efficiency by means of a prebunching region.

The relative Q and frequency separation of adjacent axial modes in tapered cavities are both significantly affected by the method of terminating the cavity. For the cavity of Fig. 1, the output coupling was assumed to be provided by a mirror of complex reflectivity R. For the results in

Fig. 5, $|R|$ was assumed to be independent of q. In fact, for highly reflecting output couplers in cavities near cutoff, it can be shown that $|R|$ is strongly dependent on q.

Assume that the cavity of Fig. (1) is terminated at $(z_0 + L)$ by free space. For a qualitative result, we may neglect mode conversion, which, however, is actually very important since $|R| \approx 1$. An approximate value of the reflectivity may be obtained from transmission line theory or by matching the RF field and its derivative at $(z_o + L)$. In either case, the result is:

$$1 - |R| \approx 2\, k_{||,0}\, k^{-1} \sim q\, \lambda L^{-1}$$

$$Q \sim 4\pi\, q^{-2}\, (L/\lambda)^3 \tag{30}$$

The dependence of $1 - |R|$ on $k_{||,0}\, k^{-1}$ is the result of diffraction of the wave near cutoff back into the waveguide, and is therefore expected to be typical for a waveguide near cutoff terminated by a low impedance output coupler. Another example which can be analyzed is termination of the cavity of Figure 1 by an output horn of angle $2\theta_2$. If we define ξ_2 by analogy to Eq.(13), and if ξ_2 is large, then, by a calculation similar to that of Eq.(22),

$$1 - |R| \approx \frac{\sqrt{3}}{2} \frac{\beta_0\, k_{||,0}\, L}{(2\xi_2)^{1/3}} \sim \frac{q\lambda}{L} \tag{31}$$

and, using Eq.(29) and assuming ξ_2 large,

$$Q \approx \frac{8}{\beta_0 \sqrt{3}} \left(\frac{L}{\lambda}\right)^2 \frac{(2\xi_2)^{1/3}}{q^2} \sim \frac{1}{q^2} \frac{L^3}{\lambda^3} \tag{32}$$

Eq.(32) was previously derived by Vlasov et al. (4).

For very high Q cavities, the expected dependence of Q is, therefore, in general,

$$Q \approx \frac{\omega L}{v_{gr}} \frac{1}{1 - |R|} \sim \frac{1}{q^2} \frac{L^3}{\lambda^3} \tag{33}$$

$$\frac{1}{v_{gr}} \sim \frac{1}{q} \frac{L}{\lambda}$$

$$\frac{1}{1 - |R|} \sim \frac{1}{q} \frac{L}{\lambda}$$

Hence the dependence of Q on q^{-2}, which is useful for mode separation, is an inherent characteristic of high Q cavities near cutoff. This favorable dependence on q can still possibly be achieved in lower Q cavities, but only through careful selection of parameters. For low Q cavities or for strong output coupling ($|R| \ll 1$), mode selectivity will, in general, be reduced. However, as noted in Section 3, in cases where a gradual taper is employed, mode selectivity may also be enhanced by allowing higher Q modes to tunnel out of the tapered end of the cavity. Other mode spoiling techniques may also be applied.

The present results indicate that the frequency separation $\Delta\omega$ of adjacent axial modes, as shown in Fig. 5, decreases with ξ. This is to be expected since, as ξ decreases, the RF-field extends further into the taper. This increases the effective cavity length, reduces $k_{\|,0}$ and the frequency separation $\Delta\omega$, and increases the cavity Q. A useful quantity for evaluating $\Delta\omega$ is:

$$\frac{\Delta\omega}{\omega} Q \frac{2}{3\pi} \longrightarrow \begin{matrix} 0.57 & \xi \to 0 \\ 1.11 & \xi \to \infty \end{matrix}$$

This quantity, which is unity for an untapered circular cylinder cavity, varies slowly with ξ, having the indicated limiting values for large and small ξ. Thus, the frequency separation of adjacent axial modes in a tapered cavity is comparable to that for untapered cavities. For moderate tapers, the frequency separation is actually somewhat reduced.

The parameter ξ is effectively a scale parameter for categorizing tapered cavities. For weakly tapered cavities, $\xi << 1$, the taper length must be very long to provide cutoff for the wave. Such long tapers, however, may be inconvenient to construct. If the taper is terminated before the wave is cutoff, the wave will be partially reflected at the end of the cavity, thus significantly changing the cavity properties. Examples of cavities with very low ξ values are, in Ref. 3, $\xi = 0.0093$, and Ref. 6, $\xi = 0.17$. For moderately tapered cavities, with ξ between about 0.3 and 3, the required taper length is modest. The present results for the axial distribution of the RF field should apply qualitatively. Examples of ξ in this range are found in Refs. 6 and 8. In fact, in Ref. 8, the results for Q vs. taper angle show, at small angles, a $\xi^{-1/3}$ dependence as predicted by the present theory. The E-field distributions obtained in Ref. (8) are also in good agreement with the present theory. For highly tapered cavities, $\xi > 40$, the tapered section acts as a mirror.

5. Conclusions

An analytic theory has been developed for treating a resonator consisting of a straight section joined to a weakly tapered section. Explicit results have been obtained for the eigenfrequencies, Q and RF-field distribution of the TE_{mpq} modes for the special case of a straight section of circular cross-section joined to a section with a linear down-taper. The results are found to be a function of the dimensionless parameter, ξ, and of L/λ, where L is the straight section length. These cavities are found to provide an axial distribution of RF-field which is useful for prebunching the electron beam and enhancing efficiency. For high Q cavities, the cavity Q is found to go as q^{-2}, which is useful for mode discrimination. Proper selection of taper length is also found to be useful for reducing the Q of high q modes. The frequency separation of modes differing only in axial mode number is comparable to that of untapered cavities, and is, in fact, somewhat reduced for weak or moderate tapers. The present results are in good qualitative agreement with previous numerical calculations (4,8).

The explicit results obtained here apply specifically to a cavity with a circular cross-section and a linear downtaper. However, the present approach should also be applicable to other weakly irregular cavities. Extension to non-circular cross-sections is straightforward since the transverse and longitudinal equations for $\vec{E}$, Eqs.(3) and (4), are solved separately. Extension to non-linear tapers can be done using WKB theory.

Such non-linear tapers have the advantage of reducing reflection and mode conversion at the taper. Mode conversion into modes which are not well confined in the resonator can be a problem since it lowers the Q and can result in leakage of the radiation toward the electron gun.

Acknowledgments

The author would like to thank K.E. Kreischer for helpful discussions and suggestions on various aspects of the present work. He would also like to thank D. Stone of Varian and M. Caplan of Hughes for very useful discussions on the theory of tapered gyrotron resonators and for discussions of unpublished numerical results.

References

1. V.A. Flyagin, A.V. Gaponov, M.I. Petelin and V.K. Yulpatov, I.E.E.E. Trans. Microwave Theory and Tech. MTT-25 (1977) 514.

2. H.R. Jory, F.I. Friedlander, S.J. Hegji, J.P. Shively and R.S. Symons, Proc. 7th Symp. Eng. Prob. Fusion Res. (1977).

3. M.E. Read, R.E. Gilgenbach, R.F. Lucey, Jr., K.R. Chu, A.T. Drobot and V.L. Granatstein, I.E.E.E. Trans. Microwave Theory and Tech. MTT-28 (1980) 875.

4. S.N. Vlasov, G.M. Zhislin, I.M. Orlova, M.I. Petelin and G.G. Rogacheva, Radiophys. and Quantum Electron. 12 No. 8 (1969) 972.

5. A.V. Gaponov, A.L. Gol'denberg, D.P. Grigor'ev, T.B. Pankratova, M.I. Petelin and V.A. Flyagin, Radiophys. and Quantum Electron. 18, No. 2 (1975) 204.

6. S.Hegji, H. Jory and J. Shively, "Development Program for a 200 kW, cw, 28 GHz Gyroklystron," Quarterly Report No. 5, Varian Associates Report No. ORNL/SUB-76/01617/5, (June, 1977) 21.

7. R.J. Temkin and S.M. Wolfe, "Design Study for a 200 GHz Gyrotron," M.I.T. Plasma Fusion Center Research Report PFC/RR-78-9 (March, 1978).

8. K.W. Arnold, J.J. Tancredi, M. Caplan, K.W. Ha, D.N. Birnbaum, and W. Weiss, "Development Program for a 200 kW, cw Gyrotron," Quarterly Report No. 3, Hughes Aircraft Company, Electron Dynamics Division Report No. ORNL/SUB-33200/3 (March, 1980).

9. R.A. Waldron, "Theory of Guided Electromagnetic Waves," Van Nostrand Reinhold Co., London (1969).

10. R.A. Waldron, Radio and Electronic Engr. 32 (1966) 245.

11. L.A. Vaynshteyn, "Open Resonators and Open Waveguides" Golem Press, Boulder, Colorado (1969).

12. R.E. Collin, "Foundations for Microwave Engineering," McGraw-Hill Book Co. New York (1966).

13. K.E. Kreischer, "High Frequency Gyrotrons and Their Application to Tokamak Plasma Heating," M.I.T. Plasma Fusion Center Research Report PFC/RR-81-1 (Jan., 1981).

14. L.I. Schiff, "Quantum Mechanics" McGraw-Hill, New York (1955).

15. A. Yariv, "Quantum Electronics" John Wiley and Sons, New York, (1975).

16. Yu. V. Bykov and A.L. Gol'denberg, Radiophys. and Qu. Electron. 18 (1975) 791.

17. G.S. Nusinovich and R.E. Erm, Elektronnaya Tekh., Ser. 1, Elektron. SVCh, No. 8 (1972) 55.

Figure Captions

Fig. 1 A model tapered gyrotron cavity consists of a straight section of length L and circular cross-section of radius R_o joined to a linearly tapered section with taper angle θ. The location of the turning point, $z = o$, varies with the resonator mode, TE_{mpq}. A partially reflecting mirror is at $(z_o + L)$.

Fig. 2 Typical values of ξ vs. θ are shown for cavities with $L/\lambda = 3,5$ and 8 and for a TE_{02q} mode.

Fig. 3 The dimensionless quantities $k_{||,o} L$ and $Q/[(4/3)\ 4\pi\ (L/\lambda)^2]$ are plotted vs. ξ (scale range 0 to 2.0) and vs. 10ξ (scale range 0 to 20) for a TE_{mpq} mode, $q = 1$, for the cavity of Fig. 1. As described in the text, results are not valid for $\xi > 5$.

Fig. 4 Same as Fig. 3, but $q = 2$. Results are valid for all values of ξ shown.

Fig. 5 The dimensionless quantities plotted vs ξ and 10ξ are $(\Delta\omega/\omega)(8L^2/\lambda^2)$, where $\Delta\omega$ is the frequency difference between a TE_{mp1} and a TE_{mp2} mode, and the ratio of the Q's of the same modes, $Q\ (q = 1)/Q\ (q = 2)$, for the cavity of Fig. 1.

Fig. 6 The normalized RF E-field distributions are plotted vs. axial distance for resonators with $\xi = 0.5$ and 5.0 and for the lowest axial modes, $q = 1$ and $q = 2$.

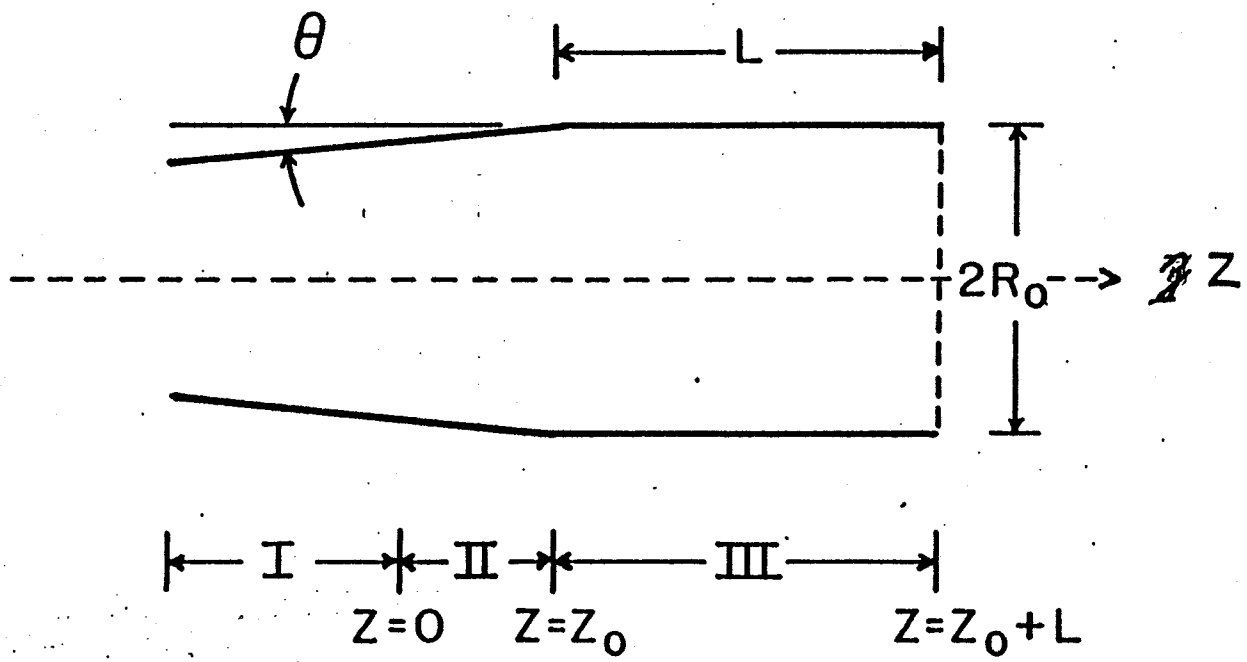

Fig. 1

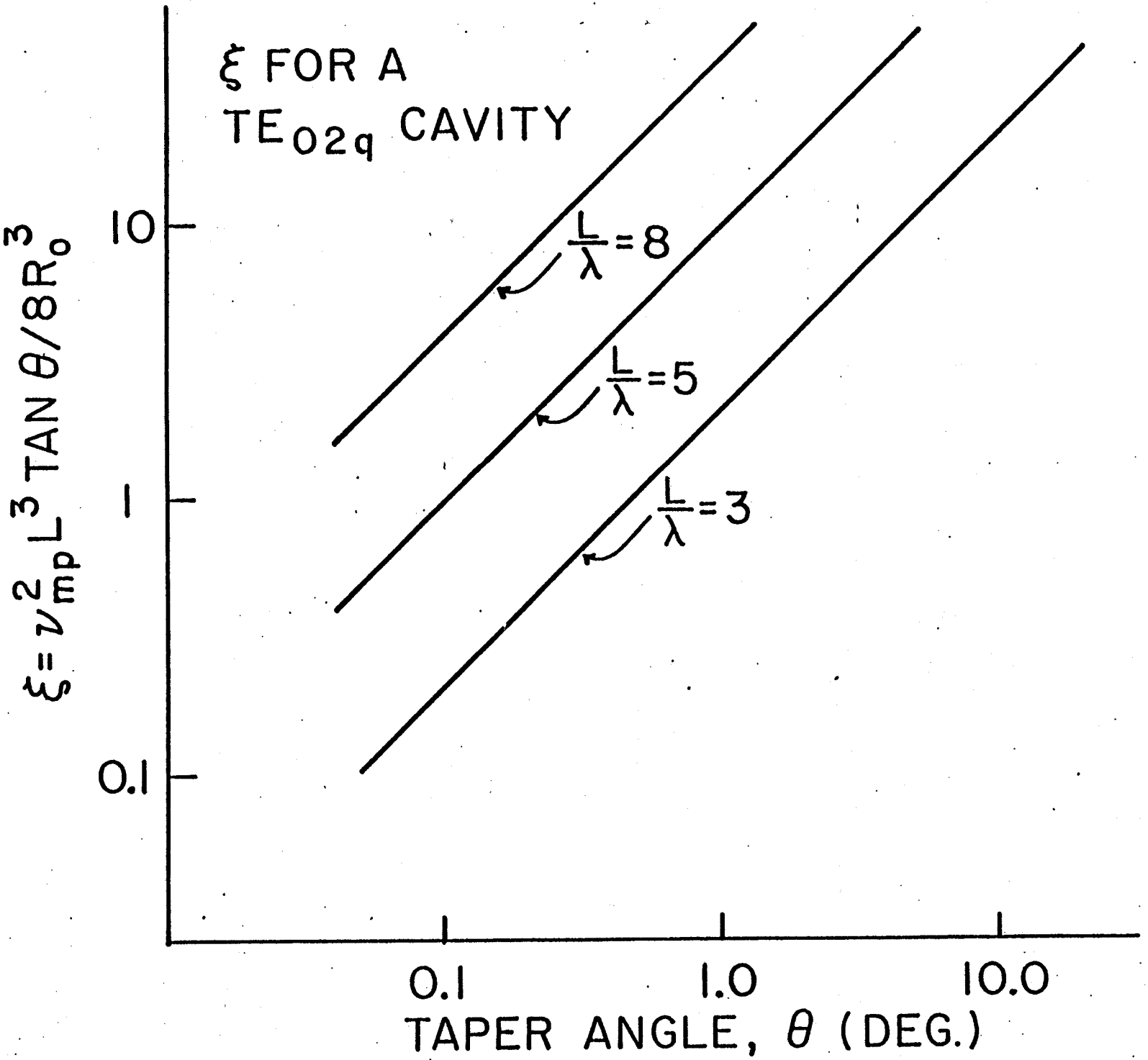
ξ FOR A
TE02q CAVITY
L/λ=8
L/λ=5
L/λ=3
10
1
0.1
ξ= νmp2L3 TAN θ/8R0 3
0.1
1.0
10.0
TAPER ANGLE, θ (DEG.)

Fig. 2

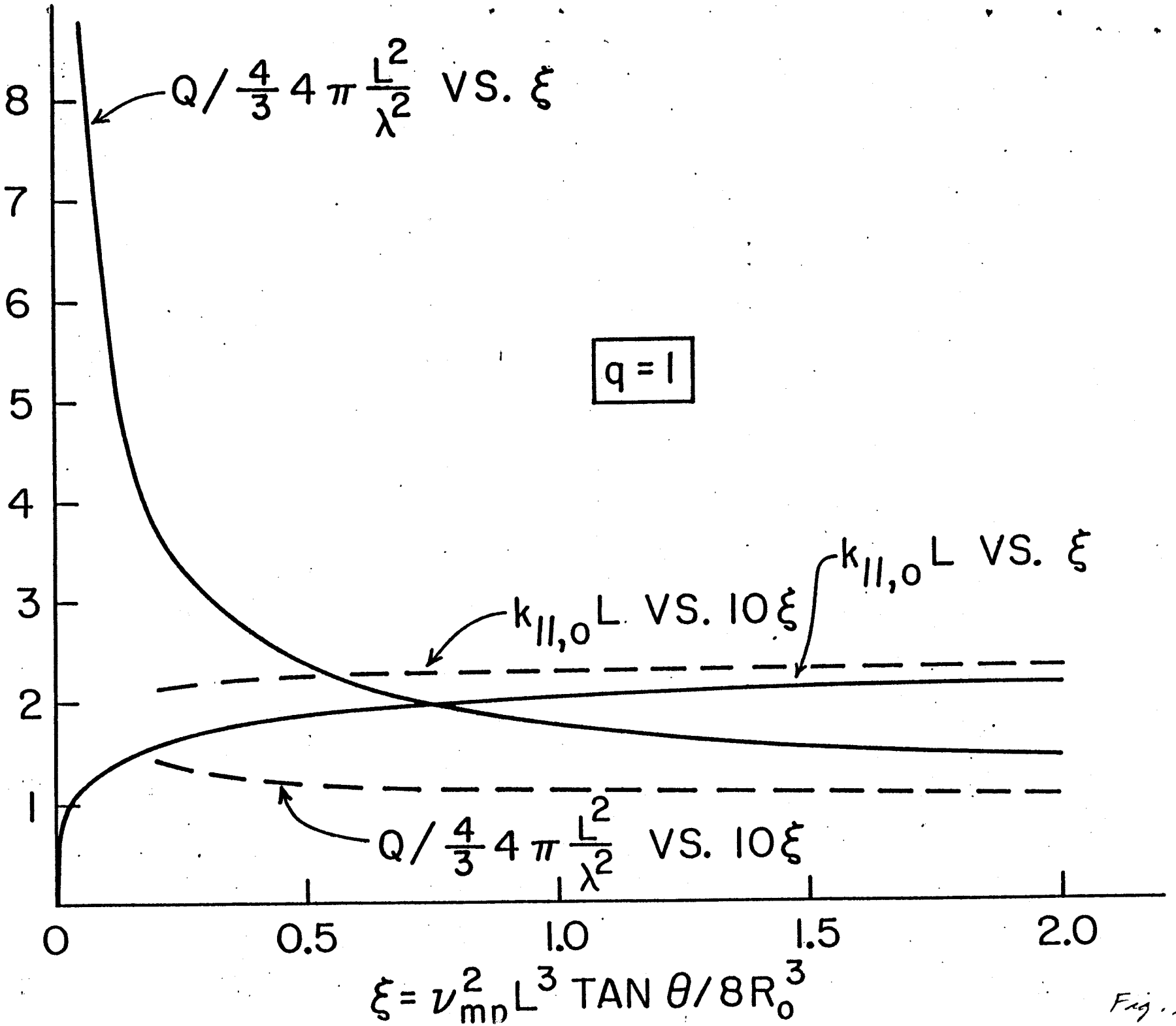
$Q/\frac{4}{3}4\pi\frac{L^2}{\lambda^2}$ VS. ξ
q = 1
$k_{11,o}L$ VS. ξ
$k_{11,o}L$ VS. 10ξ
$Q/\frac{4}{3}4\pi\frac{L^2}{\lambda^2}$ VS. 10ξ
8
7
6
5
4
3
2
1
0
0.5
1.0
1.5
2.0
$\xi = \nu_{mp}^2 L^3 \text{ TAN } \theta / 8R_o^3$

Fig. 3

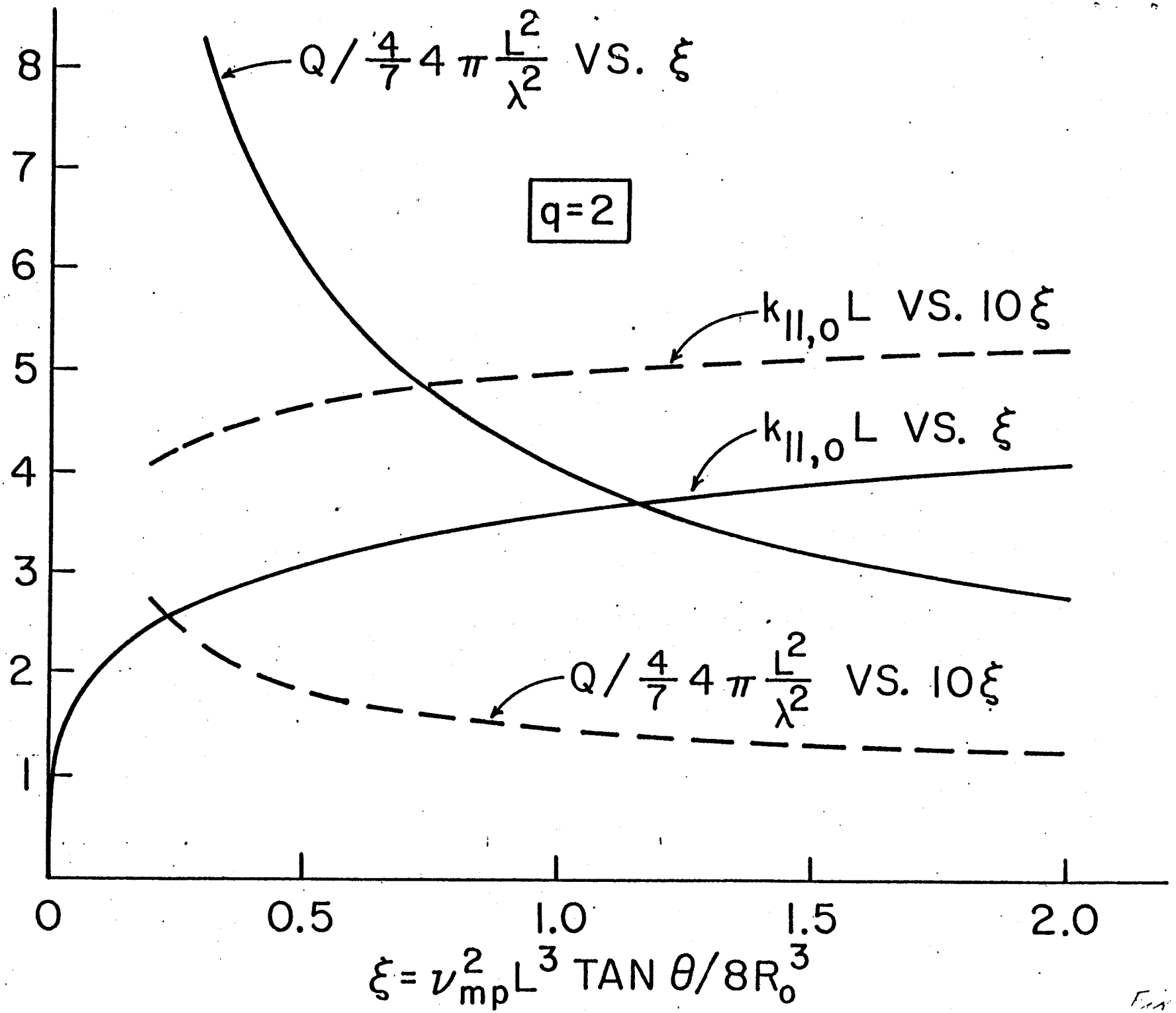
$Q/\frac{4}{7}4\pi\frac{L^2}{\lambda^2}$ VS. ξ
q=2
$k_{11,o}L$ VS. 10ξ
$k_{11,o}L$ VS. ξ
$Q/\frac{4}{7}4\pi\frac{L^2}{\lambda^2}$ VS. 10ξ
8
7
6
5
4
3
2
1
0
0.5
1.0
1.5
2.0
$\xi = \nu_{mp}^2 L^3 \text{ TAN } \theta / 8R_o^3$

Fig 4

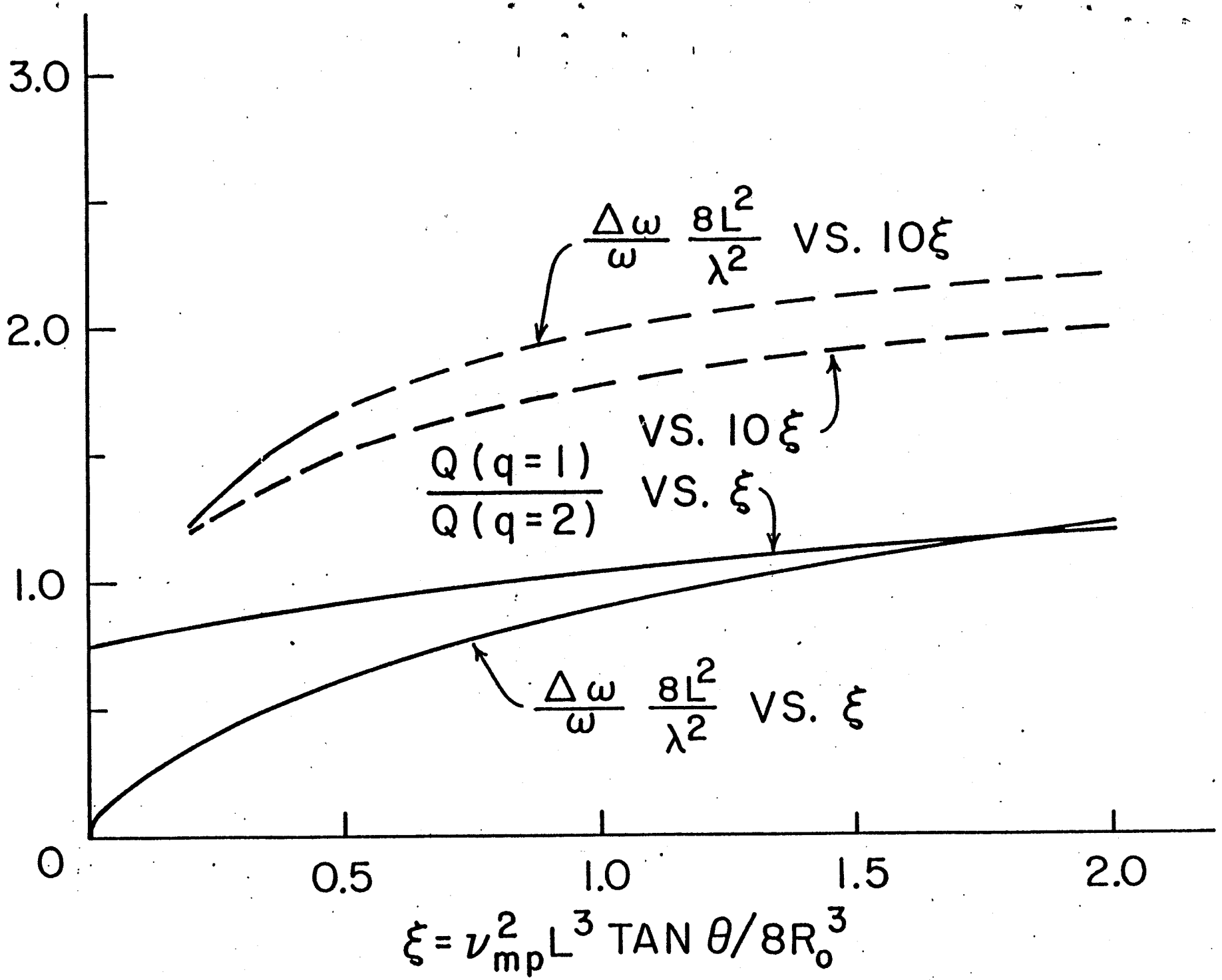
3.0
2.0
1.0
0
0.5
1.0
1.5
2.0
$\frac{\Delta\omega}{\omega}\frac{8L^2}{\lambda^2}$ VS. 10ξ
$\frac{Q(q=1)}{Q(q=2)}$ VS. 10ξ
$\frac{Q(q=1)}{Q(q=2)}$ VS. ξ
$\frac{\Delta\omega}{\omega}\frac{8L^2}{\lambda^2}$ VS. ξ
$\xi = \nu_{mp}^2 L^3 \text{ TAN } \theta / 8R_o^3$

Fig. 5

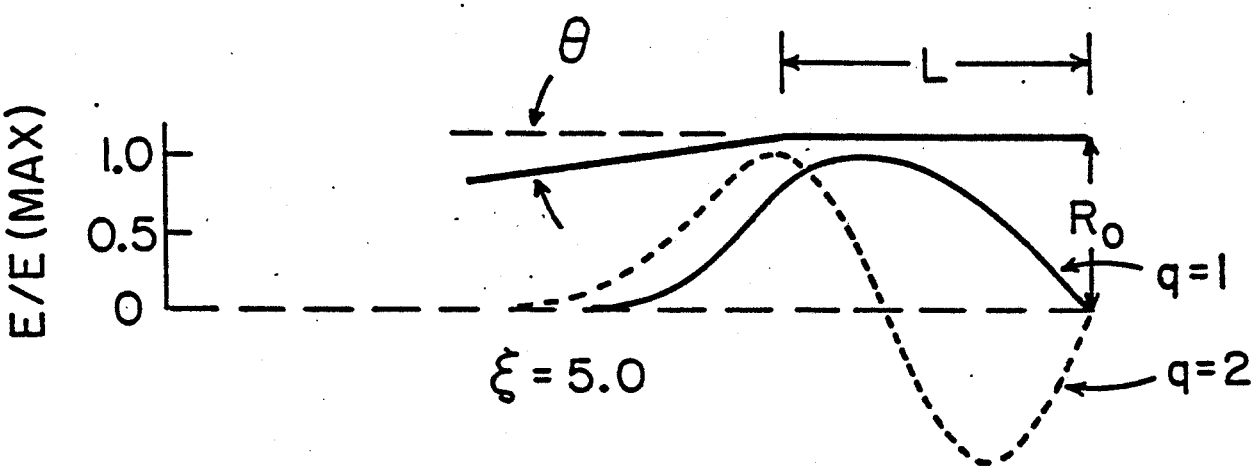
θ
L
E/E (MAX)
1.0
0.5
0
R_o
q=1
q=2
ξ = 5.0

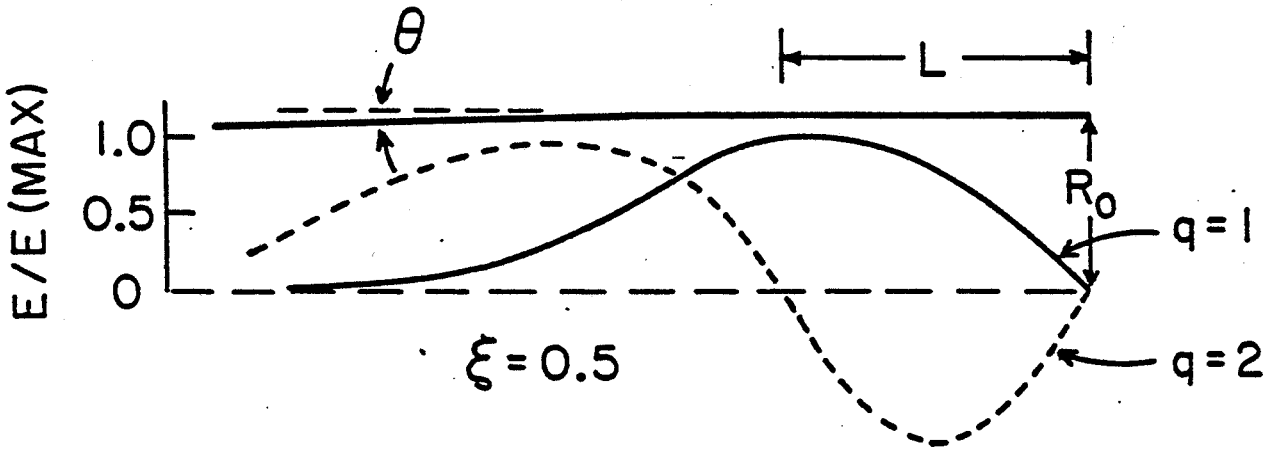
θ
L
E/E (MAX)
1.0
0.5
0
R_o
q=1
q=2
ξ = 0.5